

**Microwave, infrared-microwave double resonance, and theoretical studies of C<sub>2</sub>H<sub>4</sub>H<sub>2</sub>S complexa)**

M. Goswami, J. L. Neill, M. Muckle, B. H. Pate, and E. Arunan

Citation: *The Journal of Chemical Physics* **139**, 104303 (2013); doi: 10.1063/1.4819787

View online: <http://dx.doi.org/10.1063/1.4819787>

View Table of Contents: <http://scitation.aip.org/content/aip/journal/jcp/139/10?ver=pdfcov>

Published by the [AIP Publishing](#)

---



## Re-register for Table of Content Alerts

Create a profile.



Sign up today!



# Microwave, infrared-microwave double resonance, and theoretical studies of $C_2H_4 \cdots H_2S$ complex<sup>a)</sup>

M. Goswami,<sup>1,2,b)</sup> J. L. Neill,<sup>2</sup> M. Muckle,<sup>2</sup> B. H. Pate,<sup>2</sup> and E. Arunan<sup>1</sup>

<sup>1</sup>Department of Inorganic and Physical Chemistry, Indian Institute of Science, Bangalore 560012, India

<sup>2</sup>Department of Chemistry, University of Virginia, McCormick Road, Charlottesville, Virginia 22904, USA

(Received 10 June 2013; accepted 14 August 2013; published online 9 September 2013)

In this manuscript, rotational spectra of four new isotopologues of the S–H  $\cdots \pi$  bonded  $C_2H_4 \cdots H_2S$  complex, i.e.,  $C_2D_4 \cdots H_2S$ ,  $C_2D_4 \cdots D_2S$ ,  $C_2D_4 \cdots HDS$ , and  $^{13}CCH_4 \cdots H_2S$  have been reported and analyzed. All isotopologues except  $C_2D_4 \cdots HDS$  show a four line pattern whereas a doubling of the transition frequencies was observed for  $C_2D_4 \cdots HDS$ . These results together with our previous report on the title complex [M. Goswami, P. K. Mandal, D. J. Ramdass, and E. Arunan, Chem. Phys. Lett. **393**(1–3), 22–27 (2004)] confirm that both subunits ( $C_2H_4$  and  $H_2S$ ) are involved in large amplitude motions leading to a splitting of each rotational transition to a quartet. Further, the results also confirm that the motions which are responsible for the observed splittings involve both monomers. Molecular symmetry group analysis, considering the interchange of equivalent H atoms in  $H_2S$  and  $C_2H_4$  could explain the observed four line pattern and their intensities in the microwave spectrum. In addition, hydride stretching fundamentals of the complex were measured using coherence-converted population transfer Fourier Transform Microwave-infrared (IR-MW double resonance) experiments in the S–H and C–H stretch regions. Changes in the tunneling splittings upon vibrational excitation are consistent with the isotopic dependence of pure rotational transitions. A complexation shift of 2.7–6.5  $cm^{-1}$  has been observed in the two fundamental S–H stretching modes of the  $H_2S$  monomer in the complex. Vibrational pre-dissociation in the bound S–H stretch has been detected whereas the instrument-limited line-shapes in other S–H and C–H stretches indicate slower pre-dissociation rate. Some local perturbations in the vibrational spectra have been observed. Two combination bands have been observed corresponding to both the S–H stretching fundamentals and what appears to be the intermolecular stretching mode at 55  $cm^{-1}$ . The tunneling splitting involved in the rotation of  $C_2H_4$  unit has been deduced to be 1.5 GHz from the IR-MW results. In addition, *ab initio* barrier heights derived for different motions of the monomers support the experimental results and provide further insight into the motions causing the splitting. © 2013 AIP Publishing LLC. [<http://dx.doi.org/10.1063/1.4819787>]

## I. INTRODUCTION

Preliminary microwave investigations on  $C_2H_4 \cdots H_2S$  complex and its three other isotopologues, i.e.,  $C_2H_4 \cdots D_2S$ ,  $C_2H_4 \cdots HDS$ , and  $C_2H_4 \cdots H_2^{34}S$  revealed that the structure of the complex had S–H  $\cdots \pi$  hydrogen bond.<sup>1,2</sup> Moreover, each transition was split into two doublets with unequal splitting. The smaller splitting was less than a MHz and the larger splitting was several MHz for the  $J = 2 \rightarrow 3$  transitions. The larger splitting was absent for HDS which suggested that it could be due to the interchange of indistinguishable H/D in  $H_2S/D_2S$ . The smaller splitting exhibited an interesting trend on isotopic substitution of  $H_2S$  in the complex. As the smaller splitting persisted in the  $C_2H_4 \cdots HDS$  complex, it was attributed to internal motion within the  $C_2H_4$  subunit. The splitting was very similar for complexes with  $H_2S$  and  $H_2^{34}S$ ,

about 0.130 MHz. Also, for the complexes with HDS and  $D_2S$  it was similar, but significantly smaller than that for the  $H_2S$  isotopologues, at 0.035 MHz. In the former two cases, there is S–H  $\cdots \pi$  bonding and in the latter two cases, there is S–D  $\cdots \pi$  bonding, i.e., for the  $C_2H_4 \cdots HDS$  complex, only D bonded conformer was observed. It is well known for the complexes containing HDS<sup>3</sup> and HDO<sup>4</sup> that the D bonded conformer is more stable than the H bonded conformer largely due to the zero point energy differences. These observations were used to conclude that the smaller splitting was due to internal motion in  $C_2H_4$ , which is coupled to the S–H/S–D stretching. Clearly, experimental results on complexes with  $C_2D_4$ ,  $^{13}CCH_4$ , and IR-MW double resonance studies can provide direct confirmation of the roles of  $C_2H_4$  and  $H_2S$  in the large amplitude motions leading to the splittings. These results are presented in this manuscript.

The four line pattern observed for  $C_2H_4 \cdots H_2S$  consisted of rotational transitions having different intensities. Molecular symmetry group analysis<sup>5,6</sup> assuming the interchange of two indistinguishable H atoms in  $H_2S$  and the four H atoms in  $C_2H_4$  could explain the intensity pattern observed for the parent  $C_2H_4 \cdots H_2S$  and  $C_2H_4 \cdots D_2S$  complex. The intensities of

<sup>a)</sup>Microwave experiments and the theoretical calculations were done at Department of Inorganic and Physical Chemistry, Indian Institute of Science and the Infrared-Microwave double resonance experiments were done at Department of Chemistry, University of Virginia, Charlottesville, USA.

<sup>b)</sup>Author to whom correspondence should be addressed. Electronic mail: mausumig@gmail.com

the four lines for  $C_2D_4 \cdots H_2S/D_2S$  complexes could be predicted before these transitions were actually observed. This provided additional motive for collecting the microwave spectrum of  $C_2D_4$  complexes. Detailed molecular symmetry group analysis for the title complex is presented in this manuscript. Moreover, Bykov *et al.* have noted that the infrared spectrum of  $H_2S$  monomer has strong overtone and combination bands<sup>7</sup> and it would be interesting to see if these bands could be observed for the  $C_2H_4 \cdots H_2S$  complex. Lifetime of these weakly bound complexes show dramatic variation based on the nature of vibrational excitation even when the total vibrational energies are comparable, i.e., they exhibit clear non-RRKM (Rice-Ramsperger-Kassel-Marcus) behaviour.<sup>8</sup> The Pate group has been interested in rotational-vibrational state specific IVR (Intramolecular vibrational energy Redistribution)<sup>9,10</sup> and IR-MW double resonance studies on  $C_2H_4 \cdots H_2S$  was of natural interest.

Arunan and co-workers have been interested in complexes containing  $H_2O/H_2S$  with a primary motive of fundamental understanding of intermolecular interactions, in particular hydrogen bonding and van der Waals interaction. A detailed knowledge of the potential energy surface of the  $H_2S$  complexes is essential to understand the microscopic difference between  $H_2O$  and  $H_2S$  or more generally that of the first row and the second row hydrides. Rotational spectra provide important information about the near-equilibrium geometry and dynamics of these weak complexes. As, for example, microwave spectroscopic study of  $Ar \cdots H_2S$ <sup>3,11</sup> and  $Ne \cdots H_2S$ <sup>12</sup> complexes exhibits an unusual isotopic effect due to the presence of large amplitude motions. This is an indicator of the floppier potential of  $Ar \cdots H_2S$  compared to  $Ar \cdots H_2O$ .<sup>13</sup> Relative to the weakly bound complexes of  $H_2O$ , data on  $H_2S$  complexes are rare. Moreover, there are very few complexes where  $H_2S$  has been found to act as a hydrogen bond donor. To the best of our knowledge,  $OC \cdots H_2S$ ,<sup>14</sup>  $C_6H_6 \cdots H_2S$ ,<sup>15</sup>  $C_6H_5CCH \cdots H_2S$ ,<sup>16</sup> indole  $\cdots H_2S$ ,<sup>17</sup> 3-methylindole  $\cdots H_2S$ ,<sup>17</sup> and  $(H_2S)_2$ <sup>18,19</sup> are the only examples to have the  $H_2S$  as a hydrogen-bond donor. Though,  $OC \cdots H_2S$  is very loosely bound, microwave data indicated that the S–H group is closer to the C end of CO. Microwave investigations on  $(H_2S)_2$  showed  $H_2S$  to be effectively spherical in the complex due to the presence of large amplitude motions and hence the presence of S–H  $\cdots$  S could not be confirmed unambiguously.<sup>18</sup> A recent vacuum ultraviolet (VUV) ionization-detected IR-predissociation spectroscopic studies of  $(H_2S)_2$  indicate a redshift of  $31 \text{ cm}^{-1}$  for the hydrogen bonded S–H stretch in the complex.<sup>19</sup> Though, an earlier theoretical report on  $C_2H_4 \cdots H_2S$  complex emphasized on the presence of C–H  $\cdots$  S interaction,<sup>20</sup> preliminary microwave investigation on  $C_2H_4 \cdots H_2S$  from our group revealed that the structure is  $\pi$ -bonded with one of the hydrogen of  $H_2S$  pointing towards the  $\pi$  cloud of ethylene.<sup>1</sup> The proposed structure is very similar to the complexes of  $C_2H_4$  with other first row and second row hydrides such as  $HF$ ,<sup>21</sup>  $HCl$ ,<sup>22</sup> and  $H_2O$ .<sup>23,24</sup> Hydrogen-bond radii for  $H_2S$  has been evaluated mostly based on the theoretical data.<sup>25,26</sup> Hydrogen bond radii for other HX ( $X = F, Cl, Br, OH$ ) was determined from a large volume of experimental data available for the complexes involving them

as hydrogen bond donor. Experimental data on the complexes, where S–H group acts as a hydrogen bond donor, are essential for the semi-empirical evaluation of the hydrogen bond radii of  $H_2S$ .

## II. EXPERIMENTAL AND THEORETICAL METHODS

A cavity pulsed nozzle Fourier Transform Microwave (FTMW) spectrometer at IISc Bangalore, described elsewhere, was used to record the pure rotational spectra.<sup>27</sup> Since we published our preliminary results on the title complex, a few more transitions for the parent and  $C_2H_4 \cdots HDS$ ,  $C_2H_4 \cdots H_2^{34}S$  isotopologues were observed. In addition, rotational spectra of the isotopologues having  $C_2D_4$  and  $^{13}CCH_4$  were recorded. Inclusion of multiple FID (free induction decay) acquisition facilitated the observation of the new transitions. For  $C_2D_4 \cdots H_2S$ , about 1%–2% of  $C_2D_4$  and  $H_2S$  were seeded into argon and the mixture was expanded from a backing pressure of 0.5 bar to undergo supersonic expansion. A microwave pulse of  $0.5 \mu s$  duration was used to polarize the sample.  $HDS/D_2S$  signals were observed by passing  $H_2S$  through  $HDO/D_2O$ . Identities of the  $D_2S$  signals were confirmed by passing  $H_2S$  through a mixture of 50%  $H_2O/D_2O$ , which diminished  $C_2H_4 \cdots D_2S/C_2D_4 \cdots D_2S$  signals significantly because of the relative higher concentration of  $HDS$  in the expansion. Relative increase in  $HDS$  concentration was confirmed by monitoring the  $Ar \cdots HDS$  and  $Ar \cdots D_2S$  signals at 10 232.764 and 10 235.280 MHz, respectively.<sup>11</sup> Samples, i.e., Ar (99.999%),  $C_2H_4$  (99.9%), and  $H_2S$  (99.5%) were obtained from Bhuruka Gases Ltd. and were used without any further purification. The spectra for  $^{13}CCH_4 \cdots H_2S$  and  $C_2H_4 \cdots H_2^{34}S$  were observed in natural abundances. Isotopically enriched samples were used for  $C_2D_4$  (99 at.% D, Aldrich) and  $D_2O$  (99.95 at.% D, Aldrich).

Coherence-converted population transfer (CCPT) Fourier transform microwave-infrared spectroscopic studies on the complex were performed at University of Virginia to understand the effect of S–H and C–H stretch excitations on the band origins corresponding to the tunneling states observed by pure microwave spectroscopy. A detailed description of the experimental technique can be found in Refs. 28 and 29. The instrument is a Balle-Flygare-type FTMW spectrometer with the nozzle (1 mm pinhole, General Valve) oriented perpendicular to the cavity axis, and tuned to the frequency of a pure rotational transition of the  $C_2H_4 \cdots H_2S$  complex. A sequence of two MW pulses (each 500 ns duration) separated by 50 ns was used to excite the gas sample. The phase and amplitude of the two pulses are tuned using an arbitrary function generator (AFG) so that the first pulse is a “ $\pi/2$ ” pulse (creates the optimal pure rotational signal) and the second pulse is a “ $-\pi/2$ ” pulse, which, in the absence of a laser resonance, nulls the pure rotational signal to nearly zero. For the experiment, 80% Ne and 20% Helium were used as carrier gases. An Nd-YAG pumped OPO/OPA (Optical parametric oscillator/amplifier) tunable pulsed IR laser (Continuum Mirage) was used to excite the S–H or C–H stretch during the delay between the microwave pulses. The laser linewidth is  $\sim 0.02 \text{ cm}^{-1}$ , with a typical output power of 10 mJ/pulse at  $3000 \text{ cm}^{-1}$ , and 6 mJ/pulse at  $2600 \text{ cm}^{-1}$ . A plane parallel

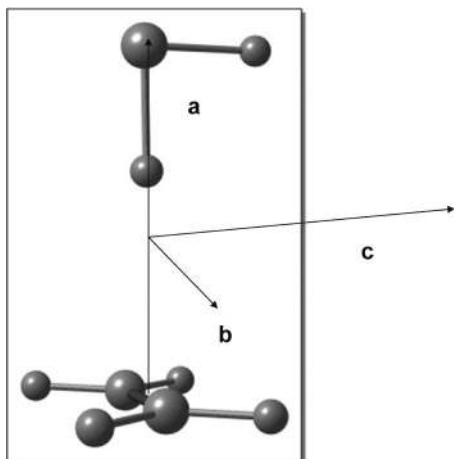


FIG. 1. Optimized geometry of  $C_2H_4 \cdots H_2S$  at MP2(full)/aug-cc-pVTZ level of theory. The optimized structure has  $C_1$  symmetry. Principal axes system of  $C_2H_4 \cdots H_2S$  is shown. Structural parameters are provided in the supplementary material.<sup>39</sup>

multipass cell was used to increase the effective path length of the IR beam inside the FTMW cavity ( $\sim 15$  passes). When the laser is resonant with a transition originating from one of the two levels involved in the transition being monitored by the FTMW cavity, a new population difference is created which is converted into a rotational coherence by the second microwave pulse. The phase of the laser-prepared coherence depends on the level from which the laser has removed population (the sign of the population difference). The measurements presented in this manuscript were done by monitoring each of the four tunneling components of the pure  $2_{02}-3_{03}$  microwave transition. The laser is typically scanned at a speed of  $0.003 \text{ cm}^{-1}/\text{s}$ . The laser and pulsed nozzle both operate at 10 Hz repetition rates, and for each data point 20 signal averages are performed (with processing time, about  $0.01 \text{ cm}^{-1}$  per data point). The scans were also performed for the  $2_{11}-3_{12}$  and  $2_{12}-3_{13}$  transitions but the signal to noise ratio was much weaker for the  $K_a = 1$  transitions.

All the calculations were performed using Gaussian 98<sup>30</sup> or Gaussian 03<sup>31</sup> program packages. Frequency cal-

culations were done to ensure that the obtained stationary points were true minima. Anharmonic calculations of the frequencies were done at MP2(full)/aug-cc-pVDZ level. Two point extrapolation formula<sup>32</sup> was used to get the binding energy at complete basis set (CBS) limit at MP2(full) level. For this purpose, single point calculation was done for the MP2(full)/aug-cc-pVDZ level optimized geometry at MP2(full)/aug-cc-pVTZ level and the binding energy at the CBS limit was determined to be  $-0.65 \text{ kcal/mol}$ . Optimized geometry of the complex at MP2(full)/aug-cc-pVTZ level is shown in Figure 1. Structural parameters and binding energies using different basis sets are provided in the supplementary material.<sup>39</sup>

Potential energy surface scans were performed for different motions of  $C_2H_4$  and  $H_2S$ . The reference geometry for the potential energy surface scan is shown in Figure 2(a). Structural parameters of the monomers were frozen at their optimized values during the scan. The angles  $\alpha/\beta/\gamma/\delta/\tau$  were varied at  $10^\circ$  step (refer to Figure 2(a) for the description of the coordinates) in the range  $0^\circ-360^\circ$ .  $R$ , the intermolecular separation, is defined as the distance between the sulphur and the mid-point of C-C bond. Results of the calculations at fixed  $R$  are provided in the supplementary material.<sup>39</sup> The results described here were obtained by varying one of the four  $\alpha/\beta/\gamma/\delta$  angles while keeping other angles fixed at the reference geometry. At the same time,  $R$  was varied from  $3.0-5.0 \text{ \AA}$ , at a step of  $0.1 \text{ \AA}$  at each angle. Counterpoise correction<sup>33</sup> was done at each point of the scan. Locations of the principal axes system of the two monomers are shown in Figure 2(b).

### III. RESULTS AND DISCUSSION

#### A. FTMW search and assignment

After the previous report on  $C_2H_4 \cdots H_2S$  was published, a few more  $a$ -dipole transitions were observed for the parent complex including the  $K_a = 2$  transitions for different  $J_s$ . However, no  $b$ -dipole or  $c$ -dipole transitions were seen. All

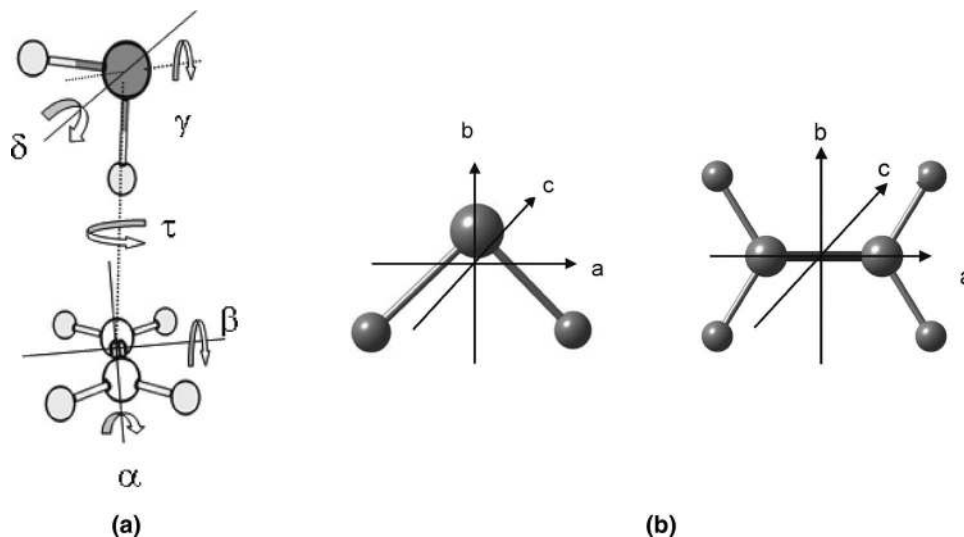


FIG. 2. (a) The reference geometry ( $\alpha = 0^\circ$ ,  $\beta = 0^\circ$ ,  $\gamma = 0^\circ$ ,  $\tau = 90^\circ$ ,  $\delta = 0^\circ$ ) of  $C_2H_4 \cdots H_2S$  complex showing the angles varied during the potential energy scans; (b) principal axes system of  $H_2S$  and  $C_2H_4$  monomer.

TABLE I. Rotational constants, centrifugal distortion constants, and standard deviation (SD) of the fits for all the four series of  $C_2H_4 \cdots H_2S$  and  $C_2D_4 \cdots H_2S$  complexes. Among two sets of doublets for each transition, the larger splitting is denoted as L–U splitting and the smaller splitting is denoted by L1–L2/U1–U2 splitting (see Figure 3).

Parameters	$C_2H_4 \cdots H_2S$				$C_2D_4 \cdots H_2S$			
	L1	L2	U1	U2	L1	L2	U1	U2
A (MHz)	25 961(34)	25 968(42)	26 189(55)	26 204(61)	17 470(12)	17 638(95)	17 572(94)	17 685(64)
B (MHz)	1972.682(2)	1972.937(2)	1974.891(3)	1975.178(3)	1822.084(3)	1822.118(2)	1822.940(2)	1822.985(2)
C (MHz)	1866.658(2)	1866.646(2)	1867.732(3)	1867.715(3)	1715.943(3)	1715.941(2)	1715.826(2)	1715.824(1)
$d_1$ (kHz)	−0.80(2)	−0.82(2)	−0.74(3)	−0.76(4)	−0.80 <sup>a</sup>	−0.82 <sup>a</sup>	−0.74 <sup>a</sup>	−0.76 <sup>a</sup>
$d_2$ (kHz)	−0.21(2)	−0.22(2)	−0.24(3)	−0.24(3)	−0.21 <sup>a</sup>	−0.22 <sup>a</sup>	−0.24 <sup>a</sup>	−0.24 <sup>a</sup>
$D_J$ (kHz)	14.30(2)	14.31(2)	13.26(3)	13.28(3)	12.2(1)	12.42(8)	11.09(8)	11.21(6)
$D_{JK}$ (MHz)	1.0587(2)	1.0575(3)	0.9691(4)	0.9684(4)	1.158(3)	1.152(3)	1.002(3)	0.998(2)
SD (kHz)	4.4	5.6	7.1	8.1	6.7	5.3	5.4	3.6
# <sup>b</sup>	17	17	17	17	9	9	9	9

<sup>a</sup>Fixed at the corresponding values for  $C_2H_4 \cdots H_2S$ .

<sup>b</sup>Number of fitted transitions.

the newly observed transitions have been fitted along with the lines reported in Ref. 1. A total of 68 transitions have been fitted into four different series using Watson's S Reduction Hamiltonian. A better fit of the rotational constants and the distortion constants was achieved for each series (Table I). All transitions for the parent complex are given in the supplementary material.<sup>39</sup> A schematic of the four line pattern observed for  $C_2H_4 \cdots H_2S$  is shown in Figure 3. Each of the rotational transitions is split into four lines—two sets of doublets separated by several MHz which is designated as L–U splitting. The smaller splitting is less than 1 MHz and denoted by L1–L2/U1–U2 splitting. More numbers of higher J transitions were also observed for  $C_2H_4 \cdots HDS$ ,  $C_2H_4 \cdots D_2S$ , and  $C_2H_4 \cdots H_2^{34}S$  isotopologues (see the supplementary material<sup>39</sup>) and a better fit for the rotational constants and distortion constants compared to Ref. 1 was achieved. The fitted parameters are listed in Tables II and III.

Predictions for  $C_2D_4 \cdots H_2S$ ,  $C_2D_4 \cdots HDS$ ,  $C_2D_4 \cdots D_2S$ , and  $^{13}CCH_4 \cdots H_2S$  isotopologues were done by putting  $H_2S$  unit as a spherical mass and by keeping the intermolecular distance fixed at 4.04 Å (the cm–cm distance derived using the isotopic data in Ref. 1). A search length of 60 MHz had to be covered to observe the  $2_{02} \rightarrow 3_{03}$  transition for  $C_2D_4 \cdots H_2S$ . Subsequent searches for  $C_2D_4 \cdots HDS$  and  $C_2D_4 \cdots D_2S$  com-

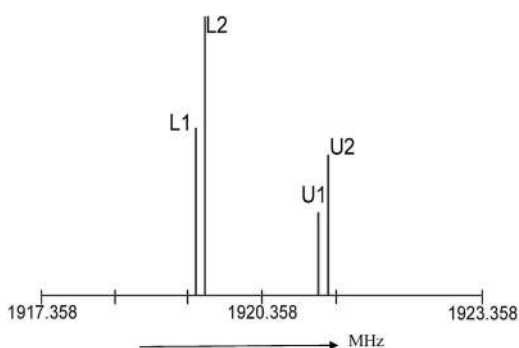


FIG. 3. A schematic of the four line pattern observed in pure MW spectra of  $C_2H_4 \cdots H_2S$  complex.  $(B + C)/2$  for each series have been plotted in the diagram.

plexes were performed by keeping this difference in mind. The transitions could be located immediately. The transition frequencies are given in the supplementary material.<sup>39</sup> Fitted parameters for  $C_2D_4 \cdots H_2S$ ,  $C_2D_4 \cdots HDS$ ,  $C_2D_4 \cdots D_2S$ , and  $^{13}CCH_4 \cdots H_2S$  complexes are listed in Tables I–IV. For complexes with  $C_2D_4$ , the smaller splitting was too small to be detected at lower J. The splittings could be resolved at higher J and it was clear that the lines were split into four components for  $C_2D_4 \cdots H_2S$  and  $C_2D_4 \cdots D_2S$  whereas lines are observed as doublets for  $C_2D_4 \cdots HDS$ . For  $^{13}CCH_4 \cdots H_2S$ , some of the transitions were too weak to be observed. The  $K_a = 1$  transitions of  $^{13}CCH_4 \cdots H_2S$  needed averaging of 10 000–15 000 gas pulses to achieve a good S/N ratio in the FTMW spectrometer (in IISc). Fitting for  $^{13}CCH_4 \cdots H_2S$  was done by keeping the A rotational constant fixed at the calculated value for the C rotational constant of  $^{13}CCH_4$  monomer. It must be noted that the A rotational constant of the parent complex is not exactly the same as the C rotational constant of ethylene monomer. For comparison, the A rotational constant of the complex is 25 961(34) MHz (L1 state) whereas the C rotational constant of the monomer is 24 864 MHz.<sup>34</sup> Scaling the calculated C rotational constant of  $^{13}CCH_4$  monomer by similar magnitude as for the parent did not improve the standard deviation of the fits for  $^{13}CCH_4 \cdots H_2S$  complex.

Hyperfine structure arising due to the quadrupole coupling of the deuterium nucleus was resolved for the  $J = 0 \rightarrow J = 1$  transitions of  $C_2H_4 \cdots HDS$  complex and are shown in Figure 4. Each of the doublets is split into three hyperfine components. Fitting of the hyperfine structures for both the series is shown in Table V. No hyperfine structures could be observed and resolved for the  $C_2D_4$  complexes.

## B. Nuclear spin statistical weights and the experimental intensities

Molecular symmetry group analyses<sup>5,6</sup> was done to obtain the nuclear spin statistical weights of the rotational-torsional levels in order to compare to the experimental intensities obtained from the microwave spectrum. The analysis was performed for three different motions of ethylene which interchanges different pairs of equivalent hydrogens in

TABLE II. Rotational constants, centrifugal distortion constants, and standard deviation (SD) of the fits for all the four series of  $C_2H_4 \cdots D_2S$  and  $C_2D_4 \cdots D_2S$  complexes. Among two sets of doublets for each transition, the larger splitting is denoted as L–U splitting and the smaller splitting is denoted by L1–L2/U1–U2 splitting (see Figure 3).

Parameters	$C_2H_4 \cdots D_2S$				$C_2D_4 \cdots D_2S$			
	L1	L2	U1	U2	L1	L2	U1	U2
A (MHz)	25 674(74)	25 580(54)	25 671(54)	25 653(48)	17.3(2)	17.5(2)	17.3(1)	17.2(1)
B (MHz)	1927.636(2)	1927.712(1)	1931.568(1)	1931.647(1)	1779.342(4)	1779.345(4)	1782.015(2)	1782.016(1)
C (MHz)	1830.274(2)	1830.264(1)	1832.560(1)	1832.524(1)	1681.589(4)	1681.583(4)	1683.022(1)	1683.017(2)
$d_1$ (kHz)	−0.52(1)	−0.54(1)	−0.62(1)	−0.63(1)	−0.80 <sup>a</sup>	−0.82 <sup>a</sup>	−0.74 <sup>a</sup>	−0.76 <sup>a</sup>
$d_2$ (kHz)	...	...	...	...	−0.21 <sup>a</sup>	−0.22 <sup>a</sup>	−0.24 <sup>a</sup>	−0.24 <sup>a</sup>
$D_J$ (kHz)	11.86(2)	11.81(2)	12.01(2)	11.99(2)	10.4(2)	10.4(1)	10.2(8)	9.96(8)
$D_{JK}$ (MHz)	0.924(1)	0.925(8)	0.904(9)	0.904(8)	1.025(5)	1.023(5)	0.978(3)	0.977(2)
SD (kHz)	3.6	2.6	2.7	2.3	10.5	9.2	5.3	4.9
# <sup>b</sup>	12	12	12	12	9	9	9	9

<sup>a</sup>Fixed at the corresponding values for  $C_2H_4 \cdots H_2S$ .

<sup>b</sup>Number of fitted transitions.

the complex. For this analysis, the equilibrium geometry of the complex was assumed to have the plane of  $H_2S$  passing through the C–C bond of  $C_2H_4$  ( $C_s$  symmetry). Orientation of the principal axis in this configuration is shown in Figure 5. The  $ac$  plane is the plane of the paper whereas the  $b$  axis is perpendicular to the plane. It is to be noted that orientation of the non-bonded hydrogen of  $H_2S$  does not alter the results obtained from this analysis

For the analysis considering the rotation of ethylene about its  $a$  axis, the feasible motions are: (1) rotation of  $C_2H_4$  about C–C bond axis; (2) internal rotation of  $H_2S$  which interchanges its equivalent hydrogens; and (3) both 1 and 2 together. Numbering of atoms is shown in Figure 5. Considering the above motions, the molecular symmetry group (MS group) consists of eight feasible operations: E, (13)(24), (56), (13)(24)(56),  $E^*$ , (13)(24)<sup>\*</sup>, (56)<sup>\*</sup>, (13)(24)(56)<sup>\*</sup>. This group is isomorphic with  $D_{2h}$  point group and is named  $G_8$  (see Table SIX of the supplementary material<sup>39</sup>). Effect of each of these operations on the equilibrium geometry of the complex is shown in Figure 5. A rotation of the complex by 180° about its  $b$  principal axis transforms each of the configurations on the right to one of those in the left, leading to four non-superimposable distinguishable minima. Hence, the rotational-torsional wave function is expected to have four-fold degeneracy.

From Figure 5, the operations (13)(24), (56),  $E^*$ , (13)(24)(56), (56)<sup>\*</sup>, (13)(24)(56)<sup>\*</sup> transform each configuration into another and thus contribute zero character to the reducible representation generated by the rotational-torsional wave function. Only operations those contribute non-zero characters are E and (13)(24)<sup>\*</sup>. In the case of  $(H_2O)_2$ , it was pointed out by Dyke<sup>35</sup> that for a prolate slightly asymmetric top, the rotational wave function transforms like  $A'$  for  $J_{even}$  and  $A''$  for  $J_{odd}$ , for  $K_a = 0$ . For  $K_a \neq 0$ , upper half of the K doublet transforms like  $A'$  for  $J_{even}$  and  $A''$  for  $J_{odd}$ . For  $K_a \neq 0$ , lower part of the K doublet transforms like  $A''$  for  $J_{even}$  and  $A'$  for  $J_{odd}$ .  $C_2H_4 \cdots H_2S$  is a nearly prolate asymmetric top with  $\kappa = -0.99$  and the above holds true for  $C_2H_4 \cdots H_2S$  as well. So, the energy level of  $C_2H_4 \cdots H_2S$  in the ground vibrational state and with  $J = 0$  ( $K_a = 0$ ),  $J = even$  ( $K_a = 0$ ),  $J = even$  ( $K = K_+$ ),  $J = odd$  ( $K = K_-$ ) will split into the following sublevels caused by the tunneling:

$$\Gamma_A' = A_1' + A_2' + B_1'' + B_2'' \quad (1)$$

Similarly, the states (in the ground vibrational state) with  $J = odd$  ( $K_a = 0$ ),  $J = odd$  ( $K = K_+$ ),  $J = even$  ( $K = K_-$ ) will split in to the following sub-levels:

$$\Gamma_A'' = A_1'' + A_2'' + B_1' + B_2' \quad (2)$$

TABLE III. Rotational constants, centrifugal distortion constants, and standard deviation (SD) of the fits for  $C_2H_4 \cdots H_2^{34}S$ ,  $C_2H_4 \cdots HDS$ , and  $C_2D_4 \cdots HDS$  complexes. Among two sets of doublets for each transition, the larger splitting is denoted as L–U splitting and the smaller splitting is denoted by L1–L2/U1–U2 splitting (see Figure 3).

Parameters	$C_2H_4 \cdots H_2^{34}S$				$C_2H_4 \cdots HDS$		$C_2D_4 \cdots HDS$	
	L1	L2	U1	U2	L1	L2	L1	L2
A (MHz)	25 920(19)	25 924(36)	25 907(58)	25 976(24)	25 877(36)	25 872(25)	17.6(1)	17.7(2)
B (MHz)	1922.905(6)	1923.146(5)	1924.764(9)	1925.0336(3)	1964.638(9)	1964.726(7)	1813.062(4)	1813.056(9)
C (MHz)	1822.019(6)	1822.009(5)	1822.819(9)	1822.8057(3)	1859.463(9)	1859.453(7)	1707.829(4)	1707.83(1)
$D_1$ (kHz)	−0.77(2)	−0.76(2)	−0.69(1)	−0.674(7)	−0.592(9)	−0.606(7)	0.6(1)	0.4(2)
$D_J$ (kHz)	13.722(7)	13.72(1)	12.60(2)	12.667(7)	11.14(1)	11.138(9)	9.3(2)	9.2(3)
$D_{JK}$ (MHz)	1.0112(2)	1.0102(4)	0.9282(6)	0.9270(3)	0.8821(6)	0.8820(5)	0.881(3)	0.879(6)
SD (kHz)	0.3	0.7	1.1	0.3	1.5	1.1	3.6	7.8
# <sup>a</sup>	9	9	9	8	10	10	8	8

<sup>a</sup>Number of fitted transitions.

TABLE IV. Fitted rotational constants, centrifugal distortion constants, and standard deviation (SD) of the fits for L1 and L2 series for  $^{13}\text{CCH}_4 \cdots \text{H}_2\text{S}$  complex. Among two sets of doublets for each transition, the larger splitting is denoted as L–U splitting and the smaller splitting is denoted by L1–L2/U1–U2 splitting. For  $^{13}\text{C}$  isotopologue, the number of lines was not enough to fit the upper series (U1/U2).

Parameters	L1	L2
A (MHz)	24 287 <sup>a</sup>	24 287 <sup>a</sup>
B (MHz)	1937.16(8)	1937.5(1)
C (MHz)	1830.9(1)	1830.8(2)
$d_1$ (kHz)	–11(2)	–12(3)
$D_J$ (kHz)	11(1)	9(2)
$D_{JK}$ (MHz)	0.95(2)	0.93(3)
SD (kHz)	84	117.0
# <sup>b</sup>	7	7

<sup>a</sup>The A rotational constant was fixed at the calculated value for the C rotational constant of  $^{13}\text{CCH}_4$  monomer.

<sup>b</sup>Number of fitted transitions.

The total wave function for  $\text{C}_2\text{H}_4 \cdots \text{H}_2\text{S}$  is antisymmetric for odd permutation of hydrogens and symmetric for their even permutation. Moreover, the effect of inversion operation on the symmetry of total wave function can be either symmetric or antisymmetric. From the  $G_8$  character table, symmetry of the total wave function for  $\text{C}_2\text{H}_4 \cdots \text{H}_2\text{S}$  was deduced to be either  $A_2'$  or  $A_2''$ . The characters for the reducible representation ( $\Gamma_{\text{NS}}$ ) formed by the nuclear spin functions of six hydrogen atoms were found using the formula:

$$\chi_p = \prod_i (2I_i + 1). \quad (3)$$

Nuclear spin functions symmetries and their degeneracies were found by reducing  $\Gamma_{\text{NS}}$  as

$$\Gamma_{\text{NS}} = 30A_1' + 10A_2' + 18B_1' + 6B_2'. \quad (4)$$

Following these, the statistical weights for the rotation-torsion states were deduced from the number of nuclear spin functions that can combine with that particular state such that the total wave function has symmetry  $A_2'$  or  $A_2''$ . The calculated statistical weights for  $\text{C}_2\text{H}_4 \cdots \text{H}_2\text{S}$ ,  $\text{C}_2\text{H}_4 \cdots \text{D}_2\text{S}$ ,  $\text{C}_2\text{D}_4 \cdots \text{H}_2\text{S}$ , and  $\text{C}_2\text{D}_4 \cdots \text{D}_2\text{S}$  isotopologues are listed in Table VI.

Considering the calculated statistical weights for  $K_a = 0$  states with  $J = \text{even}$ , the weight of  $A_1'$  state is one-third the weight for  $A_2'$  state for  $\text{C}_2\text{H}_4 \cdots \text{H}_2\text{S}$ . For  $\text{C}_2\text{H}_4 \cdots \text{D}_2\text{S}$ , the calculated weight for the  $A_1'$  state is twice that of  $A_2'$  state. The above is true for the calculated weights of  $B_2''$  and  $B_1''$  states of  $\text{C}_2\text{H}_4 \cdots \text{H}_2\text{S}$  and  $\text{C}_2\text{H}_4 \cdots \text{D}_2\text{S}$ . These ratios of 1:3 and 2:1 are reflected in the experimentally observed intensities of the lower and upper state doublets for  $K_a$

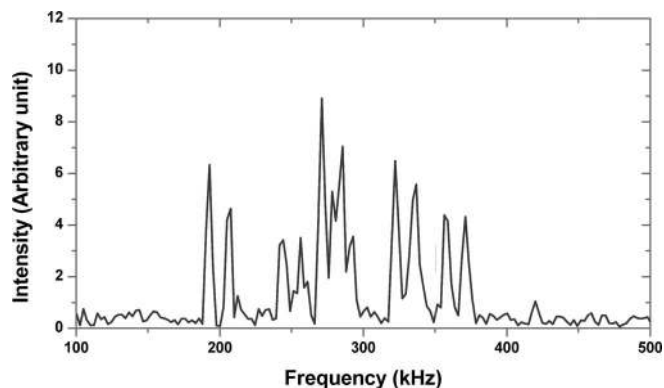


FIG. 4.  $J = 0 \rightarrow 1$  spectrum of  $\text{C}_2\text{H}_4 \cdots \text{H}_2\text{S}$  showing D quadrupole splittings, tunneling doublets, and the Doppler splittings. The spectrum was collected at 3823.8 MHz. Each component of the doublet is split into three hyperfine components which in turn are split into two Doppler components each. The spectrum was collected for 2000 gas pulses. Single FID was collected for each gas pulse. A total of 2048 points were digitized at a sampling frequency of 5 MHz.

$= 0$  lines of  $\text{C}_2\text{H}_4 \cdots \text{H}_2\text{S}$  and  $\text{C}_2\text{H}_4 \cdots \text{D}_2\text{S}$  as evident from Figures 6(a) and 6(b). Similarly, for  $\text{C}_2\text{D}_4 \cdots \text{H}_2\text{S}$ , the lower doublet is higher in intensity than the upper doublet whereas the reverse is true for  $\text{C}_2\text{D}_4 \cdots \text{D}_2\text{S}$  (see Figures SXVI and SXVII in the supplementary material<sup>39</sup>). The experimental intensity ratio of 1–2 doublets (both lower and upper) is close to 3:5 for both  $\text{C}_2\text{H}_4 \cdots \text{H}_2\text{S}$  and  $\text{C}_2\text{H}_4 \cdots \text{D}_2\text{S}$  as expected from the calculated statistical weights. For  $\text{C}_2\text{D}_4 \cdots \text{H}_2\text{S}$  and  $\text{C}_2\text{D}_4 \cdots \text{D}_2\text{S}$ , 1 and 2 (both lower and upper doublets) have equal intensity. This is expected as the calculated statistical weights for these states have a ratio of 5:4.

The analysis was also performed considering the in-plane (rotation of  $\text{C}_2\text{H}_4$  about its  $c$  principal axis) and end-over-end rotation (rotation of  $\text{C}_2\text{H}_4$  about its  $b$  principal axis) of  $\text{C}_2\text{H}_4$ . Either of these motions along with the interchange of two hydrogens of  $\text{H}_2\text{S}$  shows an eight fold degeneracy of the rotational-torsional states (see Figure SXVIII in the supplementary material<sup>39</sup>). The calculated statistical weights are the same as were deduced for the rotation of ethylene about the C–C bond axis. Though the calculated weights do not distinguish among three motions of ethylene, rotation of ethylene about the C–C bond is the only motion that reproduces the observed four line pattern in the spectra indicating the presence of this motion in the complex.

### C. Structural analysis from MW data

Substitution analysis<sup>36</sup> was employed in Ref. 1 to get an approximate zero point energy averaged structure of  $\text{C}_2\text{H}_4 \cdots \text{H}_2\text{S}$  using HDS/ $\text{D}_2\text{S}/\text{H}_2^{34}\text{S}$  isotopologue rotational

TABLE V. Fitted hyperfine transitions for  $\text{C}_2\text{H}_4 \cdots \text{H}_2\text{S}$  along with the fitted value of quadrupole coupling constant  $\chi_{\text{aa}}(\text{D})$  (projection of  $\chi_{\text{xx}}$  on dimer's  $a$  axis) for the two series.

$J'$	J	$F'$	F	Observed (MHz)	Res. (kHz)	$\chi_{\text{aa}}(\text{D})$ (kHz)	Observed (MHz)	$\chi_{\text{aa}}(\text{D})$ (kHz)	Res. (kHz)
0	1	1	0	3824.0851	0.4		3824.1640		0.3
0	1	1	2	3824.0497	–0.7	–114(2)	3824.1286	–115(1)	–0.5
0	1	1	1	3823.9993	0.3		3824.0773		0.2

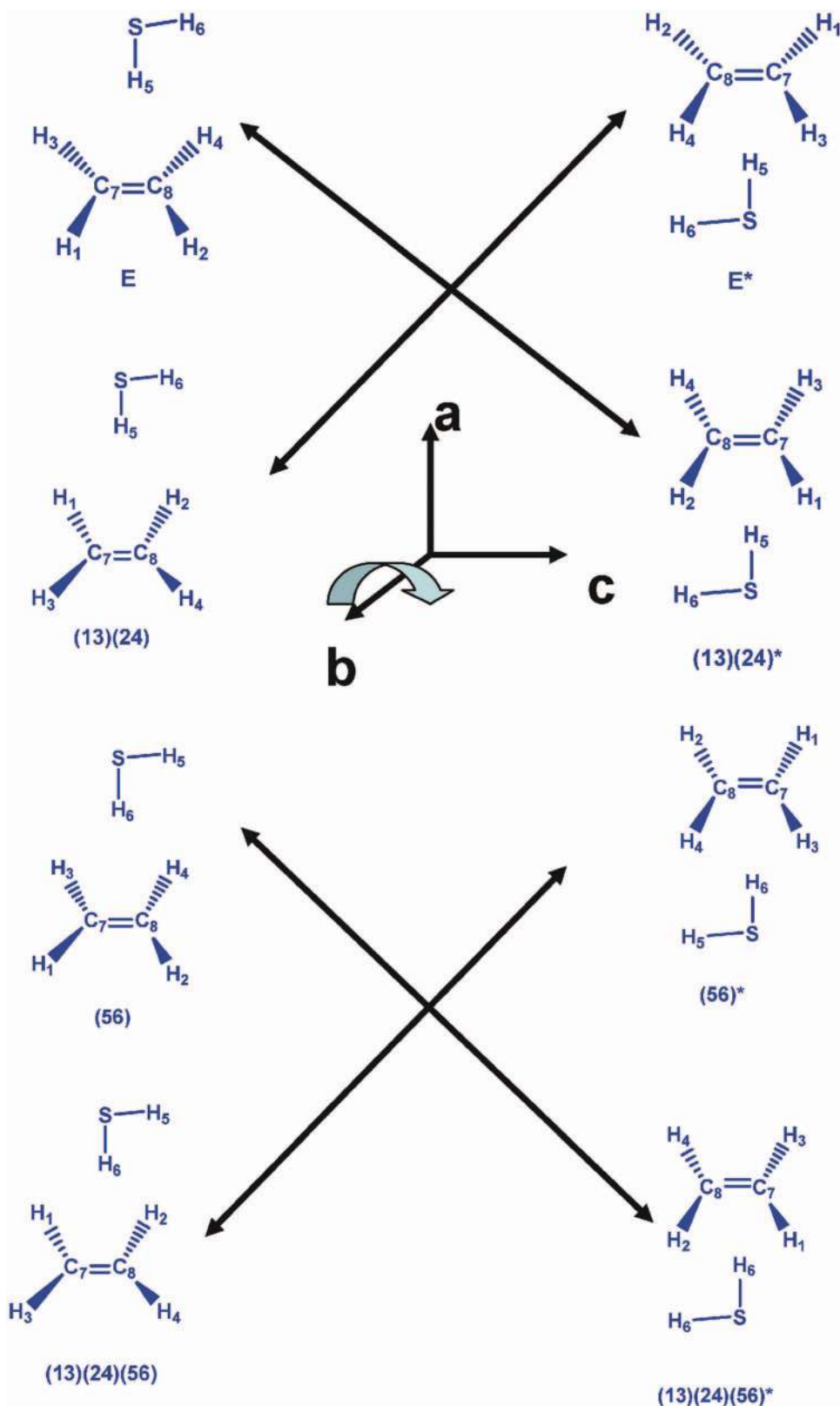


FIG. 5. Results of each MS group operation on the  $C_2H_4 \cdots H_2S$  complex are shown for the analysis, the equilibrium geometry was assumed to have  $C_s$  symmetry where the plane of  $H_2S$  contains the  $C-C$  bond. Orientation of the principal axis for this geometry is shown at the center of the figure. The configurations linked by arrows are convertible to one another by a rotation of the complex about its  $b$  principal axis.

constants. From the substitution coordinates, it was evident that only one hydrogen atom is pointing towards the  $\pi$  cloud of  $C_2H_4$ . Distance of the carbon atom from the center of mass of the complex can be derived using  $^{13}C$ -isotopologue in a

similar way and is calculated to be 2.395 Å. Also, the principal axes coordinates for the carbon atom are deduced as  $|a| = 2.086$  Å,  $|b| = 0.993$  Å,  $|c| = 0.634$  Å. The  $a$  coordinates of S (taken as the distance of the S atom from the center of

TABLE VI. Symmetry labeling of the rotational-torsional states and their spin statistical weights for  $C_2H_4 \cdots H_2S$  and its isotopologues.

Rotational-torsional sublevel symmetry	$C_2H_4 \cdots H_2S$	$C_2H_4 \cdots D_2S$	$C_2D_4 \cdots H_2S$	$C_2D_4 \cdots D_2S$
$A_1'$	10	60	45	270
$A_2'$	30	30	135	135
$B_1''$	18	18	108	108
$B_2''$	6	36	36	216
$A_1''$	10	60	45	270
$A_2''$	30	30	135	135
$B_1'$	18	18	108	108
$B_2'$	6	36	36	216

mass of the complex and was calculated as  $1.852 \text{ \AA}^1$ ) and C atom add up to  $3.938 \text{ \AA}$ ,  $0.1 \text{ \AA}$  off from the cm-cm separation in the complex. Thus, the  $a$  principal axis of the complex is not strictly parallel to the  $c$  principal axis of the ethylene monomer. The  $c$ -coordinate of  $^{13}C$  as derived above is close to half of the C–C bond distance in ethylene (experimentally determined C–C distance for  $C_2H_4$  monomer is  $1.337 \text{ \AA}^{34}$ ), which indicates that the C–C bond is lying in the  $ac$  inertial plane of the complex. However, the  $b$ -coordinate of the carbon atom is surprising. If one assumes that the  $ac$  inertial plane is passing through the C–C bond of ethylene, the  $|b|$  coordinate should be zero. This inconsistency may arise due to poorly determined rotational constants of  $^{13}CCH_4 \cdots H_2S$  complex. As was mentioned previously, the fit for  $^{13}CCH_4 \cdots H_2S$  used a fixed value for the  $A$  rotational constant of the complex. Further, it is noted that according to the *ab initio* calculated geometry of the complex, the C–C bond is lying in the  $ab$  in-

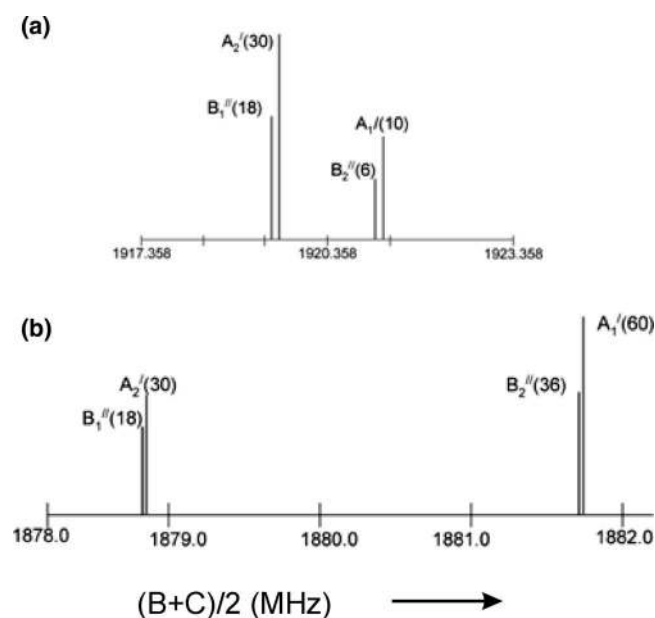


FIG. 6. Stick diagram showing the representative experimental intensity ratios for  $K_a = 0$  lines of (a)  $C_2H_4 \cdots H_2S$  and (b)  $C_2H_4 \cdots D_2S$  isotopologues. The stick diagram was generated by dividing the frequencies of  $J = 1 \rightarrow 2$  ( $K_a = 0$ ) transitions of both the complexes by  $2(J + 1)$  in order to plot with the same scale. Numbers in the parentheses are the calculated statistical weights. Note that symmetry labeling of the states is given for  $J_{\text{even}}$  (for  $K_a = 0$ ).

ertial plane (see Figure 1). A free rotation of the non-bonded hydrogen in the complex will result in an interchange of the  $b$  and  $c$  principal axes, which can also result in poorly determined  $b$ - and  $c$ -coordinates of the carbon atoms. Next, stretching force constant ( $k_s$ ) for  $C_2H_4 \cdots H_2S$  was calculated to be  $0.0191 \text{ mdyn \AA}^{-1}$ , following the method described by Aldrich, Legon, and Flygare.<sup>22</sup> For comparison, the  $k_s$  values for  $C_2H_4 \cdots H_2O^{23}$  and  $C_2H_4 \cdots HCl^{22}$  are  $0.046 \text{ mdyn \AA}^{-1}$  and  $0.066 \text{ mdyn \AA}^{-1}$ , respectively.

Hyperfine structure arising from the quadrupole coupling of the deuterium nucleus was analyzed to find out the average angle  $\theta$  of the S–D bond with the dimer  $a$  axis. This analysis was similar to what was done for  $C_6H_6 \cdots HDS$  complex.<sup>15</sup> It was assumed that the monomer geometries do not change upon complexation. For free HDS, the diagonal components of the D quadrupole interaction are  $153.7 \text{ kHz}$ ,  $-65.3 \text{ kHz}$ , and  $-88.4 \text{ kHz}$  for  $\chi_{xx}$ ,  $\chi_{yy}$ , and  $\chi_{zz}$ , respectively.<sup>37</sup> All the three hyperfine components for the  $J = 0 \rightarrow 1$  transition were fitted to a line-center to find out  $\chi_{aa}(D)$ , which is the projection of the D quadrupole interaction tensor on the dimer's inertial  $a$  axis. The fit gives  $\chi_{aa}(D)$  (projection of  $\chi_{xx}$  on dimer  $a$  axis) to be  $-114(2) \text{ kHz}$  for the lower series and  $-115(1) \text{ kHz}$  for the upper series. The average angle  $\theta$  can be found from the relation:

$$\chi_{aa} = \frac{\chi_{xx}}{2} (3 \cos^2 \theta - 1). \quad (5)$$

Using Eq. (5),  $\theta$  is calculated to be  $24.8^\circ$  for the upper state and  $24.2^\circ$  for the lower state. An almost equal magnitude of  $\theta$  for the two states of  $C_2H_4 \cdots HDS$  implies that the orientation of  $H_2S$  is similar in both the states. For  $C_6H_6 \cdots HDS$  complex,<sup>15</sup>  $\theta$  was found to be  $26^\circ$  and clearly the S–D bond orientation is similar to  $C_2H_4 \cdots HDS$ . No hyperfine transitions have been reported for  $C_2H_4 \cdots HOD$  complex whereas  $\theta$  has been derived to be  $34^\circ$  for  $C_6H_6 \cdots HOD$  complex.<sup>4</sup>

## D. Internal rotation and the isotopic dependence of the splitting

The observed transitions in MW spectra are  $a$ -dipole transitions and direction of  $a$ -dipole does not change with the rotation of ethylene or the interchange of the hydrogens of  $H_2S$ . Hence, the selection rule will connect the same tunneling levels in the lower and upper rotational states. Hence, the tunneling splittings cannot be determined from the observed rotational spectra. All the four series were fit independently using the semi-rigid rotor Hamiltonian. Difference in the rotational constants of the states can indirectly be related to the tunneling splitting. Splitting in  $(B + C)/2$  for all the isotopologues are listed in Table VII.

### 1. Smaller splitting ( $L1$ – $L2/U1$ – $U2$ )

Based on the observed changes in the smaller splitting for  $H_2S$ ,  $H_2^{34}S$ , HDS, and  $D_2S$  isotopologues, it was concluded that the smaller splitting arises due to a large amplitude motion primarily involving  $C_2H_4$  which is coupled to the bonded S–H stretch.<sup>1</sup> The new results reported in this work for  $C_2D_4$  and  $^{13}CCH_4$  are consistent with this conclusion. For

TABLE VII. Experimental splittings in  $(B+C)/2$  observed for  $C_2H_4 \cdots H_2S$  isotopologues. Among two sets of doublets for each transition, the larger splitting is denoted as L–U splitting and the smaller splitting is denoted by L1–L2/U1–U2 splitting (see Figure 3).

	1–2 (MHz)	L–U (MHz)
$C_2H_4 \cdots H_2S$	0.122(1)	1.648(2)
$C_2H_4 \cdots H_2^{34}S$	0.116(3)	1.336(2)
$C_2H_4 \cdots HDS$	0.039(4)	...
$C_2H_4 \cdots D_2S$	0.0330(8)	3.10(1)
$C_2D_4 \cdots H_2S$	0.016(1)	0.3723(8)
$C_2D_4 \cdots HDS$	0.003(4)	...
$C_2D_4 \cdots D_2S$	0.002(2)	2.053(1)
$^{13}CCH_4 \cdots H_2S$	0.1161 <sup>a</sup>	1.4938 <sup>a</sup>

<sup>a</sup>Obtained by dividing the  $2_{02} \rightarrow 3_{03}$  transition frequencies by  $2(J+1)$  as the uncertainties in the fitted rotational constants are high compared to other isotopologues.

$C_2D_4 \cdots H_2S$ , the smaller splitting shows a drastic reduction by a factor of 7 compared to the parent isotopologue. For the  $^{13}CCH_4 \cdots H_2S$ , the smaller splitting is within 5% of the parent (see Table VII). More importantly, the four-line pattern is retained for the  $^{13}CCH_4 \cdots H_2S$ . Any large amplitude motion involving interchange of the two C atoms is ruled out as that would lead to the smaller splitting vanishing. Among the three principle rotations about  $C_2H_4$ , two rotations (about its *b* and *c* axes) are ruled out. Clearly, the rotation about *a* axis of  $C_2H_4$ , which is also the C–C bond axis, causes the smaller splitting.

Comparison of the magnitude of *A* rotational constants of  $C_2H_4 \cdots HX$  ( $X = -SH, -Cl, -F$ ) complexes to that of  $C_2H_4$  also provides indication of the large amplitude motion about the C–C bond. The magnitude of *A* rotational constant of  $C_2H_4 \cdots H_2S$  is in the middle of *B* and *C* rotational constants of  $C_2H_4$  monomer. For comparison, the *A* rotational constant of the L1 state of the complex is 25 961(34) MHz whereas the *B* and *C* rotational constants of  $C_2H_4$  are 29 964 and 24 864 MHz, respectively.<sup>34</sup> The *A* rotational constant of the complex will be smaller than the *C* rotational constant of  $C_2H_4$  monomer if the  $H_2S$  molecular plane is located at  $90^\circ$  to the plane of  $C_2H_4$ . Hence, we propose that the average geometry of the title complex has a tilted  $C_2H_4$  plane due to the large amplitude rotation about the C–C bond. From previous experimental studies, the *A* rotational constants of  $C_2H_4 \cdots H_2O$ ,  $C_2H_4 \cdots HCl$ , and  $C_2H_4 \cdots HF$  are 25 857(3) (antisymmetric state),<sup>24</sup> 25 457(349),<sup>22</sup> and 24 122(13)<sup>21</sup> MHz, respectively. Thus, as we approach  $C_2H_4 \cdots H_2O$ ,  $C_2H_4 \cdots HCl$ , and  $C_2H_4 \cdots HF$ , barrier of rotation about the C–C bond of ethylene increases gradually because of a greater H bond strength compared to  $C_2H_4 \cdots H_2S$  and hence the complex shows less deviation from the mutual perpendicular orientation of the two monomers.

## 2. Larger splitting (L–U)

Results from our previous study indicated that the larger splitting vanished in  $C_2H_4 \cdots HDS$ .<sup>1</sup> Also, the splitting increased in  $C_2H_4 \cdots D_2S$  compared to  $C_2H_4 \cdots H_2S$ . Thus, it was concluded that the larger splitting is caused by a nearly

free rotation of  $H_2S$  interchanging its equivalent hydrogen atoms. It is to be noted that the change in the *A* rotational constants on  $^{34}S$  substitution is about 40 MHz for the L1–L2 states whereas the difference is about 250 MHz for the U1–U2 states. Thus, the orientation of  $H_2S$  is different in L and U states, which is precisely because the larger splitting (L–U) arises from the internal motion of  $H_2S$ .

One would expect that deuterium substitution on ethylene would not affect the larger splitting. Intriguingly, the results from the present studies indicate that the splitting decreases almost by four times in  $C_2D_4 \cdots H_2S$  compared to  $C_2H_4 \cdots H_2S$  (see Table VII). It implies that the larger splitting also has contribution from ethylene hydrogens. It is noted that a variation of the degree of splitting (caused by an interchange of equivalent hydrogens of  $H_2O$ ) on deuterium substitution of the ethylene hydrogens was also observed in case of  $C_2H_4 \cdots H_2O$ .<sup>24</sup> The larger splitting vanishes in  $C_2D_4 \cdots HDS$  as is expected. For the  $C_2D_4$  complexes, substituting  $H_2S$  with  $D_2S$  causes a further increase in the splitting like  $C_2H_4 \cdots H_2S/C_2H_4 \cdots D_2S$  complexes. However, the magnitude of this increase is much larger compared to  $C_2H_4 \cdots H_2S/C_2H_4 \cdots D_2S$  (see Table VII). The exact reason for this is beyond the scope of this study. The larger splitting remains almost unaffected ( $\sim 10\%$ ) as we substitute one of  $^{12}C$  by  $^{13}C$  as can be seen from Table VII. Thus, though the motion of  $H_2S$  is coupled to the movement of ethylene hydrogens, there is minimum involvement of the carbon atoms of  $C_2H_4$ .

## E. *Ab initio* barrier heights and the tunneling pathways

Calculated barrier heights from the potential energy surface scans and change in the radial coordinate ( $\Delta R$ ) along the minimum energy path are given in Table VIII.  $\Delta R$  gives an idea of the coupling of radial motion with the tunneling coordinate (see Sec. II for methods and Figure 2(a) for the description of other coordinates). Among the rotations of ethylene, the end-over-end rotation (rotation of  $C_2H_4$  about its *b* principal axis, i.e., change in  $\beta$ ) has the highest barrier (see Table VIII). This pathway also involves a large change in *R* (4.0–5.0 Å), which makes it highly improbable to be present in the complex. In comparison, rotation of ethylene about the C–C bond axis (its *a* principal axis, i.e., change in  $\alpha$ ) involves only a change of 0.3 Å (4–4.3 Å) in *R* and the barrier height is  $115 \text{ cm}^{-1}$  less than the end-over-end rotation. Hence, rotation about the C–C bond is more favorable and supports the experimental finding and the conclusion from MS group analysis. The in-plane rotation of ethylene (rotation about the *c* principal axis of ethylene) can be best described as rotation of  $H_2S$  about the hydrogen-bond ( $\tau$  coordinate) as the reduced mass involved in the former motion would be too high. As can be seen from Table VIII, rotation of  $H_2S$  about H bond has an extremely low barrier height (this motion is symmetric about *R* and hence, independent of *R*). However, no other state has been observed which could arise from this internal rotation. It should be mentioned that absence of any *b*- and *c*-dipole transitions in MW spectra and the observation of only *a*-type spectra in IR-MW double

TABLE VIII. Barrier for different internal motions of  $C_2H_4 \cdots H_2S$  obtained at MP2(full)/aug-cc-pVTZ level. R is the distance between the S and the mid-point of C–C bond.  $\Delta R$  = change in R along minimum energy path. See Figure 2 for description of the coordinates.

	Barrier heights ( $cm^{-1}$ )	Change in R along the minimum path ( $\text{\AA}$ )
$C_2H_4$ “a” rotation ( $\alpha$ )	361	0.3
$C_2H_4$ “b” rotation ( $\beta$ )	476	1.0
Rotation of $H_2S$ about the hydrogen bond ( $\tau$ )	10	...
$H_2S$ “b” rotation ( $\delta$ )	424	0.2
$H_2S$ “c” rotation <sup>a</sup> ( $\gamma$ )	155;468	... <sup>a</sup>

<sup>a</sup>Rotation along  $\gamma$  has two barriers. Both the barrier heights are reported. The smaller barrier ( $155\text{ cm}^{-1}$ ) is for a doubly hydrogen bonded geometry where both the hydrogens are towards ethylene ( $\gamma = 90^\circ$ ,  $\Delta R = 0$ ). The larger barrier ( $468\text{ cm}^{-1}$ ) is for the S-down configuration (when S is brought closer to the ethylene  $\pi$  cloud, oscillation in the intermolecular distance was observed along the path. The minimum energy path is no longer smooth and R was found to decrease to its minimum value of  $3.5\text{ \AA}$  (change from  $4.0\text{ \AA}$  to  $3.5\text{ \AA}$  in R, i.e.,  $\Delta R = 0.5$ ) at  $\gamma = 170^\circ$ ).

resonance (see Sec. III F) could be an indication of the presence of above motion (a free rotation of  $H_2S$  about the hydrogen bond will average out the b-dipole and c dipole to zero). The splitting may be too large to detect in our spectrometer range or the higher internal rotation levels may not be populated sufficiently in the expansion.

Experiments clearly indicated that the larger splitting arises from the interchange of two equivalent hydrogens of  $H_2S$ . Interchange of the two  $H_2S$  hydrogens can happen in two possible ways: (1) rotation of  $H_2S$  about its  $C_2$  symmetry axis (rotation about the b principal axis of  $H_2S$ , i.e., change in  $\delta$  by  $180^\circ$ ); (2) rotation of  $H_2S$  about its c principal axis (i.e.,  $\gamma$  coordinate) coupled with the rotation of  $H_2S$  about the hydrogen bond ( $\tau$ ). A  $90^\circ$  rotation of  $H_2S$  about its c principal axis together with a  $180^\circ$  rotation of  $H_2S$  about H bond will lead to an interchange of two hydrogens in  $H_2S$ . In  $C_2H_4 \cdots H_2O$ ,<sup>23</sup> the second motion was believed to interchange the hydrogen atoms of  $H_2O$  causing splitting of the rotational lines. From Table VIII, barrier for the  $90^\circ$  rotation about c axis is 3 times less than the rotation of  $H_2S$  about its  $C_2$  symmetry axis. Also, the intermolecular distance does not show any change if the  $H_2S$  unit is rotated by  $90^\circ$  about its c principal axis from the reference geometry ( $\Delta R = 0$  and  $R_{\min}$ , the value of R at which interaction energy is minimum, is at  $4.0\text{ \AA}$ ). On the other hand, rotation of  $H_2S$  about its  $C_2$  symmetry axis involves a change of R from  $4.0\text{ \AA}$  to  $4.2\text{ \AA}$ . Thus, a mechanism involving the rotation of  $H_2S$  about its c principal axis coupled with the rotation of  $H_2S$  about H bond is

more probable. However, a more definitive conclusion regarding the dynamics of  $H_2S$  motion cannot be derived from the present set of experimental data. Further, the motions which cause the splittings involve both  $C_2H_4$  and  $H_2S$  subunits and are actually coupled. Hence, these one-dimensional *ab initio* calculations serve as only a qualitative guidance to decipher the dynamics.

## F. IR-MW double resonance investigations

IR-MW double resonance studies probe the tunneling-level specific band origins in the S–H and C–H stretch regions which provide information on the coupling of the intermolecular and the intramolecular modes. Further, these studies give information on the S–H stretch shifts of the  $H_2S$  monomer upon complexation with ethylene.

### 1. S–H Stretch

Two vibrational bands corresponding to the S–H stretch fundamentals were detected for each of the four tunneling states. The S–H stretch fundamentals for the  $H_2S$  monomer are  $2614.355\text{ cm}^{-1}$  and  $2628.431\text{ cm}^{-1}$ , respectively.<sup>7</sup> Band origins for the lower and higher frequency S–H stretches in the complex are listed in Table IX. Compared to the monomer, complexation shifts of  $\sim 2.7$ – $6.5\text{ cm}^{-1}$  were observed. Both the S–H stretches exhibit purely a-type spectra. IR-MW scans for the quartets belonging to  $2_{02}$ – $3_{03}$  are shown in Figures 7(a) and 7(b). In these spectra, upward-pointing transitions originate from the higher energy rotational state ( $3_{03}$ ), while downward-pointing transitions originate from the lower energy state ( $2_{02}$ ). Evidence of vibrational pre-dissociation in the low frequency band has been seen whereas the high frequency band shows near instrumental linewidths. The slower scan ( $0.001\text{ cm}^{-1}/s$ ) shown in Figure 8 reveals a broader linewidth ( $0.05\text{ cm}^{-1}$ ) for the lower band. Thus, the lower frequency band has more contribution from the bonded S–H stretch which is coupled to the intermolecular stretch leading to pre-dissociation. In fact, a close inspection of the calculated  $H_2S$  modes in the complex reveals that the lower frequency mode has more contribution from the bonded hydrogen stretch whereas the higher frequency mode looks like a stretching of the non-bonded hydrogen of  $H_2S$ .

Calculated shifts in the S–H stretches using aug-cc-pVD(T)Z basis sets using MP2(full) method are given in Table IX (vibrational frequencies are given in Table SXIII in the supplementary material<sup>39</sup>). Theory predicts a larger redshift for the symmetric stretch compared to the asym-

TABLE IX. The first four columns report the band origins (in  $cm^{-1}$ ) for the four tunneling states observed in the S–H stretch region for  $C_2H_4 \cdots H_2S$  complex along with the experimental shifts (in  $cm^{-1}$ ) in the S–H stretches in the parentheses. All bands are a-type. Theoretical redshifts in the S–H stretches ( $\Delta\nu$  in  $cm^{-1}$ ) are reported in last two columns on the right. The frequency shifts are calculated at MP2(full) level on the counterpoise corrected surface.

L1	L2	U1	U2	Free $H_2S$ <sup>7</sup>	$\Delta\nu$ /aug-cc-pVDZ	$\Delta\nu$ /aug-cc-pVTZ
2607.88 (6.475)	2607.86 (6.495)	2608.30 (6.055)	2608.28 (6.075)	2614.355	21 (13) <sup>a</sup>	28
2622.18 (6.251)	2622.18 (6.251)	2625.72 (2.711)	2625.70 (2.731)	2628.431	9 (4) <sup>a</sup>	7

<sup>a</sup>Anharmonic frequency shifts calculated at MP2(full)/aug-cc-pVDZ level are shown in parentheses.

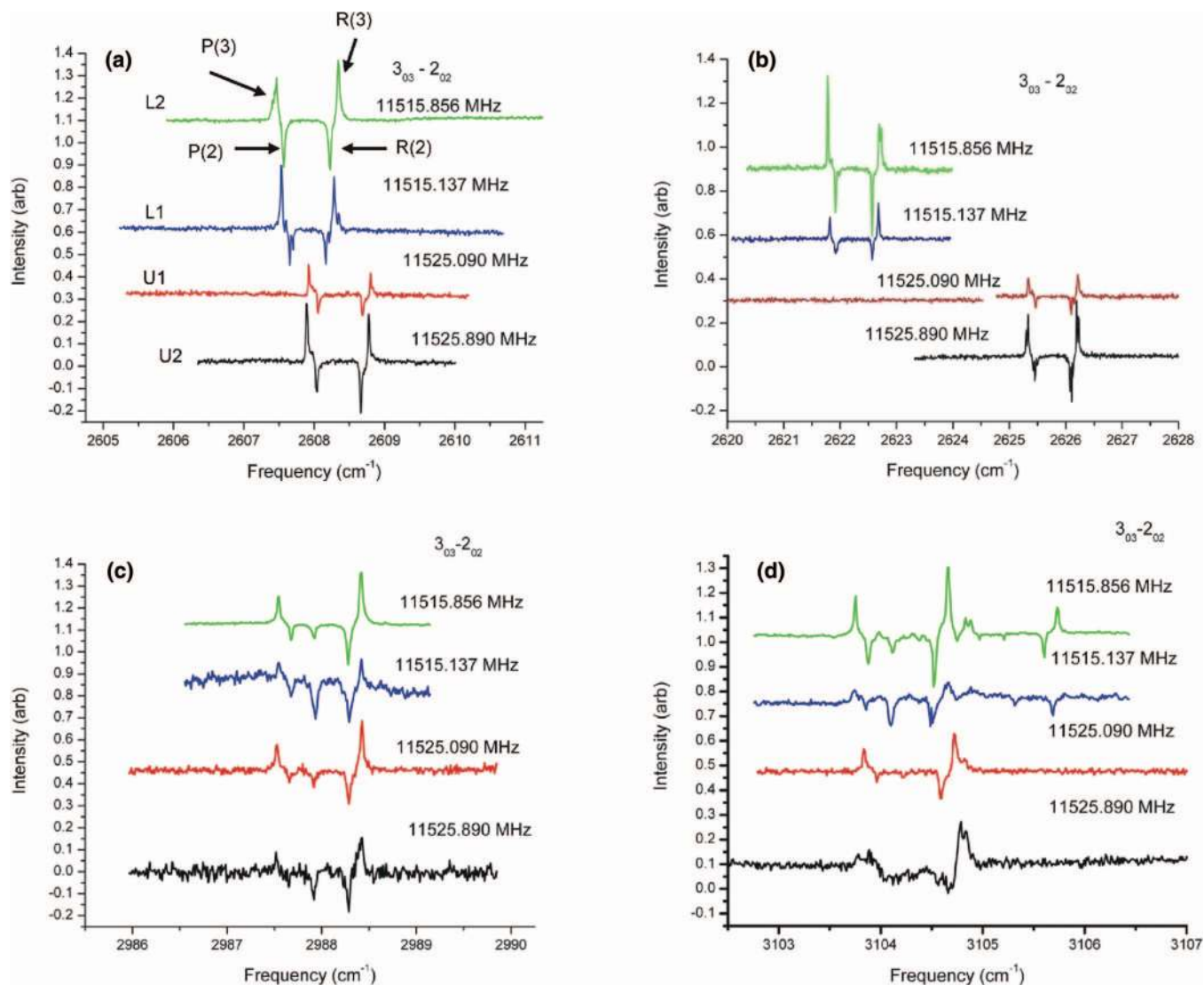


FIG. 7. IR-MW scans for  $\text{C}_2\text{H}_4 \cdots \text{H}_2\text{S}$  showing (a) bonded S-H stretch region; (b) non-bonded S-H stretch region; (c) *b* type C-H stretch; and (d) *c* type C-H stretch for each tunneling component of  $J = 2_{02} \rightarrow 3_{03}$  transitions.

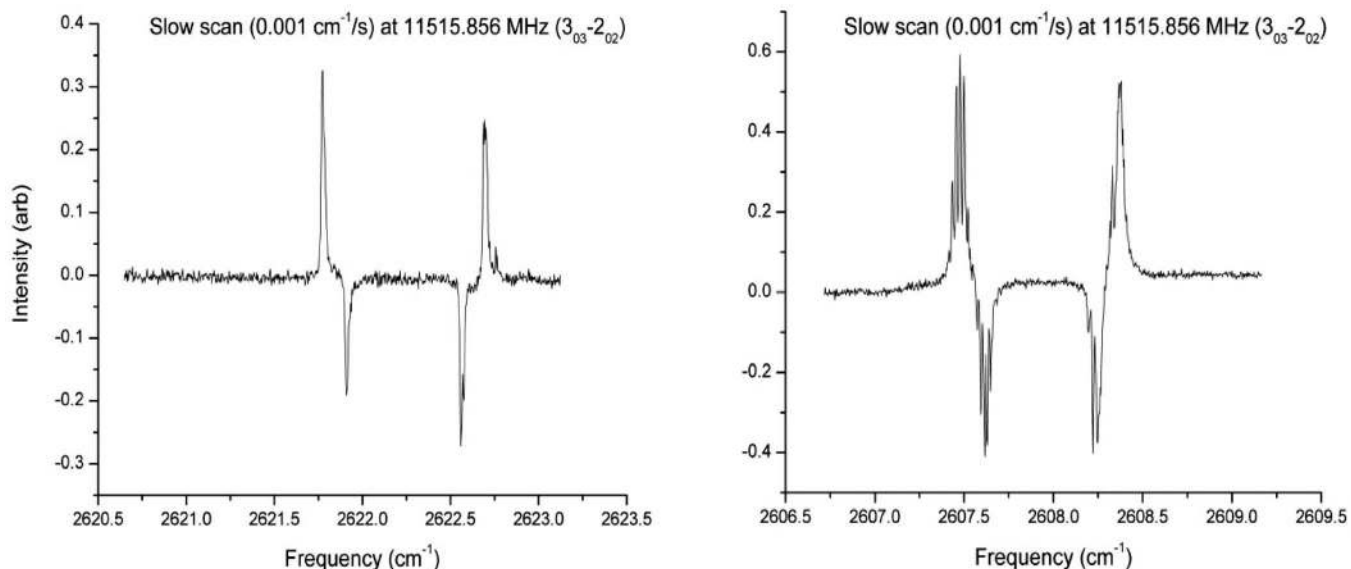


FIG. 8. IR-MW scans for  $\text{C}_2\text{H}_4 \cdots \text{H}_2\text{S}$  showing slow scan for both the S-H stretches monitored at 11 515.856 (L2,  $2_{02} \rightarrow 3_{03}$ ). Broader linewidth is observed for the low frequency band as is seen on the right hand side of the figure.

metric stretch. Anharmonic calculation at aug-cc-pVDZ level reduces the redshift by 55% and 38% for the symmetric and asymmetric stretches, respectively. It must be mentioned that the anharmonic frequency calculations identified the frequency corresponding to the rotation about the hydrogen bond as an imaginary frequency.

A close look at Table IX shows that for both the S–H stretches, 1–2 states (smaller splitting in the MW) have same band origins and the band origins differ for the L–U states (larger splitting in the MW). For comparison, band origins for the lower frequency band are 2607.88 (L1), 2607.86(L2), 2608.30(U1), and 2608.28(U2)  $\text{cm}^{-1}$ . Thus excitation in the S–H stretches causes changes in the L–U splitting (larger splitting) whereas the 1–2 splitting (smaller splitting) is similar for both the ground and excited states. This essentially means that the intermolecular mode responsible for the larger splitting is coupled to the S–H stretch. On the other hand, excitation in the S–H stretches causes little effect to the motion causing the smaller splitting. This is in agreement with the assignments from the pure MW data that the smaller splitting involves the motion of the ethylene sub-unit whereas the larger splitting is caused by the movement of the  $\text{H}_2\text{S}$  subunit.

The next important observation from Table IX is that the difference in the band origin for the L–U states is  $0.45 \text{ cm}^{-1}$  for the low frequency band and  $3.5 \text{ cm}^{-1}$  for the high frequency band. Thus the excitation in the non-bonded hydrogen of  $\text{H}_2\text{S}$  (as the higher frequency band has more contribution from the non-bonded S–H stretch) causes a greater change in the spacing of the torsional states corresponding to the  $\text{H}_2\text{S}$  motion in the complex. This greater change in the spacing may be a consequence of the coupling of the  $\text{H}_2\text{S}$  rotation about hydrogen bond to the  $\text{H}_2\text{S}$  c rotation leading to the hydrogen interchange.

One can speculate that the L–U splitting would decrease as we excite the S–H stretches in the complex. The torsional mode of  $\text{H}_2\text{S}$  which causes the L–U splitting is more like a rotation and any increase in the S–H bond length would result in an increase in the moment of inertia and hence, the spacing between the torsional levels is expected to decrease.

Two more weak a-type vibrational bands at 2663.4 and 2676.1  $\text{cm}^{-1}$  were observed 55  $\text{cm}^{-1}$  above the S–H stretch fundamentals and are assigned as the combination bands of S–H stretch and the intermolecular stretching at 55  $\text{cm}^{-1}$ . The intermolecular stretch was calculated to be 69  $\text{cm}^{-1}$  at MP2(full)/aug-cc-pVTZ level of calculation and the anharmonic calculation at MP2(full)/aug-cc-pVDZ level leads to 51  $\text{cm}^{-1}$ . Broadening similar to the lower band of the fundamental S–H stretches has been observed for the lower frequency band. A slow scan ( $0.001 \text{ cm}^{-1}/\text{s}$ ) of these bands showing the broadening has been included in the supplementary material.<sup>39</sup>

## 2. C–H Stretch

Two vibrational bands for the complex have been observed near the two infrared active fundamental C–H stretches of ethylene monomer. Frequencies of these bands

TABLE X. Band origins (in  $\text{cm}^{-1}$ ) for the four tunneling states observed in C–H stretch region for  $\text{C}_2\text{H}_4 \cdots \text{H}_2\text{S}$  complex. The lower frequency band is b-type whereas the higher frequency band is c-type.

	L1	L2	U1	U2	$\text{C}_2\text{H}_4$ band origins
b-type	2987.12	2987.12	2987.12	2987.12	2988.643 <sup>38</sup>
c-type	3103.32	3103.33	3103.42	3103.51	3104.887 <sup>38</sup>
	3103.56	3103.56			
	3104.49	3104.40			

for the monomer are 2988.643  $\text{cm}^{-1}$  and 3104.887  $\text{cm}^{-1}$ .<sup>38</sup> Experiments reveal only minor complexation shifts for these bands. *Ab initio* anharmonic frequency calculations at MP2(full)/aug-cc-pVDZ level predict a shift of 4  $\text{cm}^{-1}$  and 2  $\text{cm}^{-1}$  for the lower and higher C–H stretches, respectively. The low frequency band for the complex is b-type whereas the high frequency band is c-type. Representative IR–MW scans in the C–H stretch region are shown in Figures 7(c) and 7(d).

Band origins for the four tunneling states are listed in Table X. In case of the lower frequency band, all the four states have same band origin within the experimental resolution. Thus, exciting the lower C–H stretch has very little effect on the barriers of the intermolecular motions causing the splittings. The higher frequency band showed local Coriolis perturbation in the L1 and L2 states and the band origins were fitted to three c-type bands. The perturbations were absent for the upper tunneling states (U1–U2) and a difference of  $0.1 \text{ cm}^{-1}$  in the band origin was observed for these states. Difference in the band origin can have contribution from two factors: (1) excitation in the mode causes changes in the barrier height of the ethylene tunneling motion. (2) selection rule allows the transition to occur from 1(ground state)  $\rightarrow$  2(excited state) and 2(ground state)  $\rightarrow$  1(excited state). The latter would happen if the tunneling motion (here, the rotation of ethylene about C–C bond) changes the vibrational displacement vectors of the higher frequency C–H stretch. One can expect that excitation in the higher frequency mode will have no effect on the barrier height of ethylene rotation, similar to the low frequency mode. Vibrational displacement vectors for the low and high frequency C–H stretches of  $\text{C}_2\text{H}_4$  is shown in Figure 9. Unlike the low frequency mode, vibrational displacement vectors for the high frequency C–H stretch change with the rotation of ethylene about C–C bond axis. Thus, we conclude that shift in the band origin for the 1–2 states is mainly due to the selection rule which allows the transition

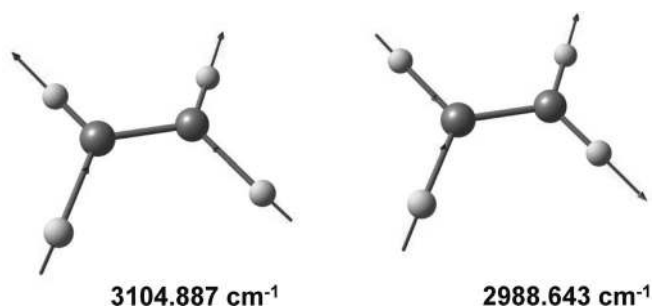


FIG. 9. Vibrational displacement vectors for the C–H stretch vibrations of  $\text{C}_2\text{H}_4$  monomer.

to connect different tunneling states in the ground and excited states. Hence, the tunneling splitting caused by the rotation of ethylene can be estimated from this data. From the given data, the tunneling splitting caused by the rotation of  $C_2H_4$  about the C–C bond is calculated as  $0.05\text{ cm}^{-1}$  (1.5 GHz).

Absence of Coriolis coupling for the U1–U2 pair signifies that these perturbations are tunneling-level specific. The coupled vibrational states may involve intermolecular excitation or the excitation within the  $H_2S$  unit, which can cause changes in the barrier for the  $H_2S$  hydrogen interchange and hence, detuning the U1–U2 pair from resonance. Also, excitation in the coupled vibrational modes does not change the barrier for the rotation of ethylene about C–C bond axis as the perturbation pattern observed in L1 and L2 is very similar.

#### IV. CONCLUSIONS

The rotational spectra of various isotopologues of  $C_2H_4 \cdots H_2S$  indicate that two large amplitude motions are present in the complex which results into four line pattern for the parent isotopologue. Both the motions can be described as coupled motion of both  $C_2H_4$  and  $H_2S$  units. The smaller splitting arises because of the internal rotation of ethylene coupled with the bonded S–H compression. Rotational spectra of  $^{13}CCH_4 \cdots H_2S$  and  $C_2D_4 \cdots H_2S$  confirm that the dynamics of ethylene in the complex, which gives rise to the smaller splitting involves the rotation about its C–C bond axis. Molecular symmetry group analysis and the *ab initio* calculations at MP2(full) level support the conclusions drawn from the experiments. Experimentally observed intensity ratios of the quartets are fairly reproduced by the molecular symmetry group analysis. The larger splitting is caused by the interchange of the  $H_2S$  hydrogens. Decrease of the larger splitting in  $C_2D_4 \cdots H_2S$  indicates the involvement of ethylene hydrogens in the dynamics causing the larger splitting. IR-MW double resonance studies in S–H and C–H stretch regions of  $C_2H_4 \cdots H_2S$  corroborate the findings by pure rotational spectroscopy. Two S–H stretch bands were detected for each of the four tunneling states. The tunneling pair arising from the ethylene motion shows the same band origin in the S–H stretch region whereas the band origins are different for the tunneling pair arising from the  $H_2S$  motion supporting the assignments from the microwave studies. Further, the data show that the bonded S–H stretch is coupled to the intermolecular stretching causing pre-dissociation broadening. Two combination bands of S–H stretch and the intermolecular stretching mode at  $55\text{ cm}^{-1}$  were observed. Two vibrational bands were observed in the C–H stretch region. The low frequency C–H stretch shows the same band origin for all the four tunneling states indicating that barrier for the intermolecular motion does not change upon C–H stretch excitation. The high frequency band showed Coriolis perturbation for the lower tunneling doublets (L1–L2) whereas the perturbation was absent for the upper tunneling pair. The displacement vector change of the high frequency C–H stretch during the ethylene C–C rotation makes it possible to determine the tunneling splitting caused by the ethylene motion, which was determined to be 1.5 GHz.

#### ACKNOWLEDGMENTS

E.A. and M.G. thank the Department of Science and Technology, India and the Indo-French Center for the Promotion of Advanced research for the financial support. We acknowledge the Supercomputer Educational Research Centre of the Indian Institute of Science for the computational facilities. M.G. acknowledges a research fellowship from the council of Scientific and Industrial Research, India. B.P. acknowledges the National Science Foundation for funding.

- <sup>1</sup>M. Goswami, P. K. Mandal, D. J. Ramdass, and E. Arunan, *Chem. Phys. Lett.* **393**(1–3), 22–27 (2004).
- <sup>2</sup>M. Goswami and E. Arunan, *Phys. Chem. Chem. Phys.* **11**(40), 8974–8983 (2009).
- <sup>3</sup>H. S. Gutowsky, T. Emilsson, and E. Arunan, *J. Chem. Phys.* **106**(13), 5309–5315 (1997).
- <sup>4</sup>H. S. Gutowsky, T. Emilsson, and E. Arunan, *J. Chem. Phys.* **99**(7), 4883–4893 (1993).
- <sup>5</sup>H. Longuet-Higgins, *Mol. Phys.* **6**(5), 445–460 (1963).
- <sup>6</sup>P. R. Bunker and P. Jensen, *Molecular Symmetry and Spectroscopy* (NRC Research Press, 2006).
- <sup>7</sup>A. D. Bykov, O. V. Naumenko, M. A. Smirnov, L. N. Sinita, L. R. Brown, J. Crisp, and D. Crisp, *Can. J. Phys.* **72**(11–12), 989–1000 (1994).
- <sup>8</sup>L. Oudejans and R. Miller, *Chem. Phys.* **239**(1), 345–356 (1998).
- <sup>9</sup>D. Green, S. Hammond, J. Keske, and B. H. Pate, *J. Chem. Phys.* **110**(4), 1979–1989 (1999).
- <sup>10</sup>D. A. McWhorter, E. Hudspeth, and B. H. Pate, *J. Chem. Phys.* **110**, 2000 (1999).
- <sup>11</sup>R. Bumgarner, D. Pauley, and S. Kukolich, *J. Mol. Struct.* **190**, 163–171 (1988).
- <sup>12</sup>Y. Liu and W. Jäger, *Mol. Phys.* **100**(5), 611–622 (2002).
- <sup>13</sup>G. Fraser, F. Lovas, R. Suenram, and K. Matsumura, *J. Mol. Spectrosc.* **144**(1), 97–112 (1990).
- <sup>14</sup>Y. Xu, P. Arboleda, and W. Jäger, *J. Mol. Spectrosc.* **229**(1), 47–53 (2005).
- <sup>15</sup>E. Arunan, T. Emilsson, H. Gutowsky, G. T. Fraser, G. De Oliveira, and C. Dykstra, *J. Chem. Phys.* **117**, 9766 (2002).
- <sup>16</sup>M. Goswami and E. Arunan, *J. Mol. Spectrosc.* **268**(1–2), 147–156 (2011).
- <sup>17</sup>H. S. Biswal and S. Wategaonkar, *J. Phys. Chem. A* **113**(46), 12774–12782 (2009).
- <sup>18</sup>F. J. Lovas, P. K. Mandal, and E. Arunan, private communication (December 2012); P. K. Mandal, Ph.D. thesis, Indian Institute of Science, 2005.
- <sup>19</sup>A. Bhattacharjee, Y. Matsuda, A. Fujii, and S. Wategaonkar, *ChemPhysChem* **14**(5), 905–914 (2013).
- <sup>20</sup>M. Hartmann, S. D. Wetmore, and L. Radom, *J. Phys. Chem. A* **105**(18), 4470–4479 (2001).
- <sup>21</sup>J. Shea and W. Flygare, *J. Chem. Phys.* **76**, 4857 (1982).
- <sup>22</sup>P. Aldrich, A. Legon, and W. Flygare, *J. Chem. Phys.* **75**, 2126 (1981).
- <sup>23</sup>K. I. Peterson and W. Klemperer, *J. Chem. Phys.* **85**, 725 (1986).
- <sup>24</sup>A. M. Andrews and R. L. Kuczkowski, *J. Chem. Phys.* **98**, 791 (1993).
- <sup>25</sup>P. K. Mandal and E. Arunan, *J. Chem. Phys.* **114**, 3880 (2001).
- <sup>26</sup>B. Raghavendra, P. K. Mandal, and E. Arunan, *Phys. Chem. Chem. Phys.* **8**(45), 5276–5286 (2006).
- <sup>27</sup>E. Arunan, A. Tiwari, P. Mandal, and P. Mathias, *Curr. Sci.* **82**(5), 533–540 (2002); available at <http://www.currentscience.ac.in/php/toc.php?vol=082&issue=05>.
- <sup>28</sup>S. Twagirayezu, T. N. Clasp, D. S. Perry, J. L. Neill, M. T. Muckle, and B. H. Pate, *J. Phys. Chem. A* **114**(25), 6818–6828 (2010).
- <sup>29</sup>J. L. Neill, K. O. Douglass, B. H. Pate, and D. W. Pratt, *Phys. Chem. Chem. Phys.* **13**(16), 7253–7262 (2011).
- <sup>30</sup>M. J. Frisch, G. W. Trucks, H. B. Schlegel, G. E. Scuseria, M. A. Robb, J. R. Cheeseman, V. G. Zakrzewski, Jr., J. A. Montgomery, R. E. Stratmann, J. C. Burant, S. Dapprich, J. M. Millam, A. D. Daniels, K. N. Kudin, M. C. Strain, O. Farkas, J. Tomasi, V. Barone, M. Cossi, R. Cammi, B. Menonucci, C. Pomelli, C. Adamo, S. Clifford, J. Ochterski, G. A. Petersson, P. Y. Ayala, Q. Cui, K. Morokuma, N. Rega, P. Salvador, J. J. Dannenberg, D. K. Malick, A. D. Rabuck, K. Raghavachari, J. B. Foresman, J. Cioslowski, J. V. Ortiz, A. G. Baboul, B. B. Stefanov, G. Liu, A. Liashenko, P. Piskorz, I. Komaromi, R. Gomperts, R. L. Martin, D. J. Fox, T. Keith, M. A. Al-Laham, Vreven, C. Y. Peng, A. Nanayakkara, M. Challacombe, P. M. W. Gill, B. Johnson, W. Chen, M. W. Wong, J. L. Andres, C. Gonzalez, M.

- Head-Gordon, E. S. Replogle, and T. J. A. Pople, Gaussian 98, Revision A.11.3 Gaussian, Inc., Pittsburgh, PA, 2002.
- <sup>31</sup>M. J. Frisch, G. W. Trucks, H. B. Schlegel, G. E. Scuseria, M. A. Robb, J. R. Cheeseman, Jr., J. A. Montgomery, T. Vreven, K. N. Kudin, J. C. Burant, J. M. Millam, S. S. Iyengar, J. Tomasi, V. Barone, B. Mennucci, M. Cossi, G. Scalmani, N. Rega, G. A. Petersson, H. Nakatsuji, M. Hada, M. Ehara, K. Toyota, R. Fukuda, J. Hasegawa, M. Ishida, T. Nakajima, Y. Honda, O. Kitao, H. Nakai, M. Klene, X. Li, J. E. Knox, H. P. Hratchian, J. B. Cross, C. Adamo, J. Jaramillo, R. Gomperts, R. E. Stratmann, O. Yazyev, A. J. Austin, R. Cammi, C. Pomelli, J. W. Ochterski, P. Y. Ayala, K. Morokuma, G. A. Voth, P. Salvador, J. J. Dannenberg, V. G. Zakrzewski, S. Dapprich, A. D. Daniels, M. C. Strain, O. Farkas, D. K. Malick, A. D. Rabuck, K. Raghavachari, J. B. Foresman, J. V. Ortiz, Q. Cui, A. G. Baboul, S. Clifford, J. Cioslowski, B. B. Stefanov, G. Liu, A. Liashenko, P. Piskorz, I. Komaromi, R. L. Martin, D. J. Fox, T. M. Keith, A. Al-Laham, C. Y. Peng, A. Nanayakkara, M. Challacombe, P. M. W. Gill, B. Johnson, W. Chen, M. W. Wong, C. Gonzalez, and J. A. Pople, Gaussian 03, Revision C-02, Gaussian, Inc., Wallingford, CT, 2004.
- <sup>32</sup>C. J. Cramer, *Essentials of Computational Chemistry: Theories and Models* (Wiley, 2005).
- <sup>33</sup>S. F. Boys and F. d. Bernardi, *Mol. Phys.* **19**(4), 553–566 (1970).
- <sup>34</sup>H. C. Allen, Jr. and E. K. Plyler, *J. Am. Chem. Soc.* **80**(11), 2673–2676 (1958).
- <sup>35</sup>T. R. Dyke, *J. Chem. Phys.* **66**(2), 492–497 (1977).
- <sup>36</sup>W. Gordy and R. L. Cook, *Microwave Molecular Spectra* (John Wiley, 1984).
- <sup>37</sup>R. Viswanathan and T. Dyke, *J. Mol. Spectrosc.* **103**(2), 231–239 (1984).
- <sup>38</sup>B. G. Sartakov, J. Oomens, J. Reuss, and A. Fayt, *J. Mol. Spectrosc.* **185**(1), 31–47 (1997).
- <sup>39</sup>See supplementary material at <http://dx.doi.org/10.1063/1.4819787> for microwave transition frequencies, *ab initio* optimized structural parameters, binding energies, vibrational frequencies, and potential energy curves, etc.